Wide-Scan Spherical-Lens Antennas for Automotive Radars

Bernhard Schoenlinner, *Student Member, IEEE*, Xidong Wu, *Student Member, IEEE*, Jim P. Ebling, George V. Eleftheriades, *Senior, Member, IEEE*, and Gabriel M. Rebeiz, *Fellow, IEEE*

***Abstract*—A new approach to wide scan-angle antennas at millimeter-wave frequencies is introduced with special focus on ease of manufacturing and reliability. The system is composed of planar feed antennas (tapered-slot antennas), which are positioned around a homogeneous spherical Teflon lens. Beam scanning can be achieved by switching between the antenna elements. The spherical-lens system is analyzed through a combined ray-optics/diffraction method. It is found that a maximum efficiency of 50%–55% can be achieved using Teflon, Rexolite, or quartz lenses. The efficiency includes taper, spillover, and reflection loss. Calculations also indicate that the maximum lens diameter is 30–40 λ_0, which results in a maximum directivity of 39.5–42 dB. Measurements done on a single-element feed and a 5-cm Teflon lens agree very well with theory and result in a 3-dB beamwidth of 5.5° and better than −20-dB sidelobe levels at 77 GHz. Absolute gain measurements show a system efficiency of 46%–48% (including dielectric loss). A 23- and 33-element antenna array with a scan angle of ±90° and a −3.5- and −6-dB crossover, respectively, in the far-field patterns was also demonstrated. The 23-element array resulted in virtually no gain loss over the entire 90° scan angle. This represents, to our knowledge, the first wide scan-angle antenna at millimeter-wave frequencies.**

***Index Terms*—Automotive radars, imaging systems, millimeter waves, planar antennas, spherical lens, tapered slot antenna, wide scan angle.**

I. Introduction

AUTOMOTIVE radars at 60 or 77 GHz are currently being developed for automatic cruise control and/or collision avoidance applications. Most systems employ 3–5 switched antenna beams using a standard focal-plane system with a collimating lens [1], [2]. A focal-plane system with f/0.9 allows the formation of 7–9 beams, but wide-angle scanning performance is limited due to off-axis aberrations.

There are several methods of achieving a wide-angle system without mechanical scanning. An excellent design is given by Demmerle *et al*. [3] using a bi-conical antenna and radial feed points, but this is applicable up to 3 GHz. Another method is the use of a Luneburg lens [4], [5], but this requires a graded dielectric lens, which is expensive to manufacture at millimeter-wave frequencies. Mossallei *et al.* recently calculated the radiation properties of a nonuniform Luneburg-lens antenna with an optimum selection of each shell thickness and dielectric constant [6]. Another solution is a two-shell spherical lens with the core of the lens focusing the optical rays and the outer shell acting as a matching layer [7], [8]. In fact, the system efficiency of 63% for the optimized five-shell Luneburg lens can also be achieved by an optimized two-shell lens design [6]. Still, a two-shell lens requires the presence of an undesirable interface and air gaps, which increases the cost of the system and can cause pattern degradation at millimeter-wave frequencies.

A single spherical lens with a homogeneous dielectric is a very practical solution for millimeter-wave applications. However, early analysis of this antenna did not take into account the effect of the feed pattern and the optimization of the location of the feed antenna [9], [10]. Also, a systematic study of the efficiency of homogeneous spherical-lens antennas has never been reported (spillover, taper, reflection). This paper shows that a homogeneous spherical dielectric lens, when well designed, results in excellent patterns and an acceptable system efficiency (around 54%). This paper also presents a low-cost solution to feeding the spherical-lens antenna, mainly by the use of planar endfire tapered slot antennas. A multibeam wide scan-angle antenna system with a scanning performance of 180° and a 3- and 6-dB pattern crossover is also presented. This paper concludes with a comparison between Teflon, Rexolite, and quartz dielectric lens antennas for wide scan-angle performance.

II. Theory

The normalized paraxial focal length of a spherical lens is given by [9]

$$\frac{\overline{FO}}{R} = \frac{n}{2(n-1)} \tag{1}$$

where n is the refractive index of the lens material. This is true when a small on-axis portion of the spherical surface is illuminated (paraxial focus). Fig. 1 shows the normalized focal length, calculated using ray-tracing techniques, as a function of the angle of plane-wave incidence for a dielectric constant of $\varepsilon_r = 2.08$ (Teflon), 2.54 (Rexolite), and 3.78 (fused quartz). For the case of quartz, the paraxial focus falls just outside the lens. The maximum angle to guarantee that the normalized focal length be greater than one (in order to ensure that the focus lies outside the lens) is 87°, 74°, and 27° for dielectric constants of 2.08, 2.54, and 3.78, respectively. Since it is desirable to have good illumination over an extended portion of the spherical lens, a small dielectric constant material should be used.

Manuscript received September 16, 2001.

B. Schoenlinner and G. M. Rebeiz are with the Radiation Laboratory, Department of Electrical Engineering and Computer Science, The University of Michigan at Ann Arbor, Ann Arbor, MI 49109-2122 USA (e-mail: bernhrd@engin.umich.edu; rebeiz@engin.umich.edu).

X. Wu and G. V. Eleftheriades are with The Edward S. Rogers Sr. Department of Electrical and Computer Engineering, University of Toronto, Toronto, ON, Canada M5S 3G4 (e-mail: xidong@waves.utoronto.ca; gelefth@waves.utoronto.ca).

J. P. Ebling is with Canopus Systems Inc., Ann Arbor, MI 48105 USA.

Publisher Item Identifier 10.1109/TMTT.2002.802331.

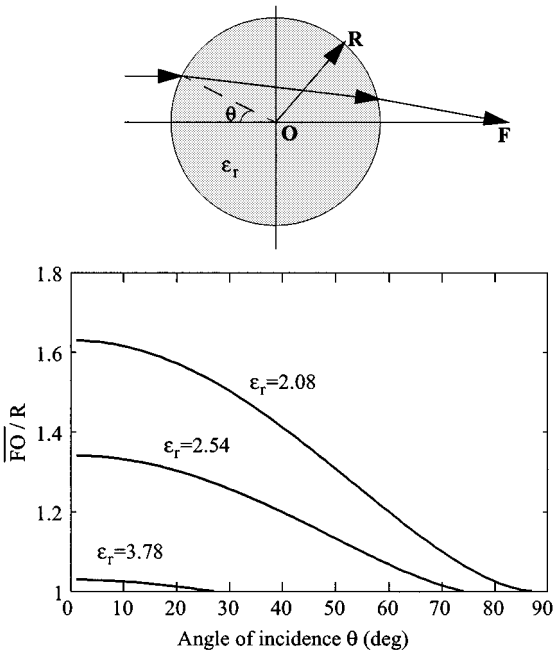

Fig. 1. Normalized focal length as a function of the angle of incidence for spherical lenses with different dielectric constants.

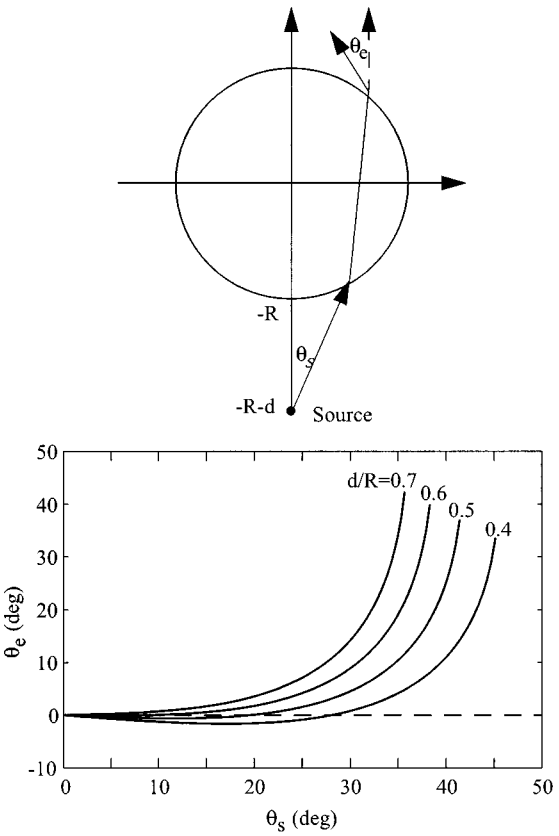

Fig. 2. Exit angle θ_e as a function of the input angle θ_s for a Teflon spherical lens for different d/R.

Fig. 2 shows the ray tracing from a point source at a distance d from the edge of a Teflon spherical lens. In order to achieve diffraction-limited patterns, which means a maximum directivity, whose limit is given by the size of the aperture (the maximum area of the lens), the exit angle θ_e should be as small as possible for all input angles θ_s. This is achieved for d/R between 0.4–0.55. Note that the optical paraxial focal position is $d/R = 0.63$ for the Teflon case. From this calculation, it is obvious that the optimal feed position for achieving maximum directivity does not coincide with the paraxial focus.

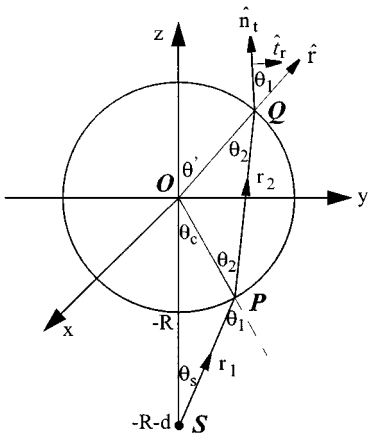

Fig. 3. Geometry used for radiation pattern calculation.

To calculate the far-field pattern, a universal class of feeds is first chosen with gain patterns defined by

$$G(\theta) = \begin{cases} 2(m+1)\cos^m\theta, & 0 \le \theta \le \dfrac{\pi}{2} \\ 0, & \dfrac{\pi}{2} < \theta \le \pi. \end{cases} \tag{2}$$

Assuming that the feed source pattern is y-polarized (see Fig. 3), the incident field pattern can be expressed as

$$\mathbf{E}^s = \hat{e}_i \sqrt{G(\theta)}\gamma \tag{3}$$

where $\hat{e}_i$ is a unit vector perpendicular to $\hat{r}$ ($\hat{r}$ is the radial unit vector) and parallel to the plane formed by $\hat{r}$ and $\hat{y}$ and is

$$\hat{e}_i = (\hat{r} \times \hat{y}) \times \frac{\hat{r}}{\sin\psi} = \frac{(\hat{y} - \cos\psi\hat{r})}{\sin\psi} \tag{4}$$

where ψ is the angle between $\hat{r}$ and $\hat{y}$. The electric-field components can then be written as

$$\begin{aligned} E^s_\theta &= (\hat{e}_i \cdot \hat{\theta})|E^s| \\ &= \frac{\cos\theta\sin\phi}{\sqrt{1-\sin^2\theta\sin^2\phi}}\sqrt{2(m+1)}\cos^{m/2}\theta \end{aligned} \tag{5}$$

$$\begin{aligned} E^s_\phi &= (\hat{e}_i \cdot \hat{\phi})|E^s| \\ &= \frac{\cos\phi}{\sqrt{1-\sin^2\theta\sin^2\phi}}\sqrt{2(m+1)}\cos^{m/2}\theta. \end{aligned} \tag{6}$$

For a −10-dB beamwidth of 80°, $m = 9$ and the directivity is 13 dB.

The geometry of the problem is shown in Fig. 3. In this case, each ray encounters two diffractions before escaping out of the spherical lens, i.e., the first one from the source point S to the first trace point P and then from point P to the second trace point Q (see Fig. 3). In order to solve the ray-tracing problem, first the maximum value of the input angle θ_s is defined accor-

ding to

$$\theta_s \le \theta_m = \sin^{-1}\left(\frac{R}{R+d}\right). \tag{7}$$

The other pertinent angles in Fig. 3 can then be expressed in terms of θ_s as follows:

$$\theta_1 = \sin^{-1}\left(\frac{\sin\theta_s}{\sin\theta_m}\right) \tag{8}$$

$$\theta_c = \theta_1 - \theta_s \tag{9}$$

$$\theta_2 = \sin^{-1}\left(\frac{\sin\theta_1}{n}\right) \tag{10}$$

$$\theta' = 2\theta_2 - \theta_c. \tag{11}$$

The perpendicular and parallel polarization components of the electric field at point Q outside the lens are

$$E_\perp = E_\phi^s \frac{e^{-jk_0 r_1}}{r_1} T_\perp(P) e^{-jk_0 n r_2} \cdot \mathrm{DF} \cdot T_\perp(Q) \tag{12}$$

$$E_\parallel = E_\theta^s \frac{e^{-jk_0 r_1}}{r_1} T_\parallel(P) e^{-jk_0 n r_2} \cdot \mathrm{DF} \cdot T_\parallel(Q) \tag{13}$$

where E_ϕ^s and E_θ^s are the source field patterns, as found from (5) and (6). Furthermore, $T_\perp$ and $T_\parallel$ are the perpendicular and parallel Fresnel transmission coefficients at points P, Q, respectively. Also, r_1, r_2 are the distances from point S to point P and from point P to point Q, respectively,

$$r_1 = \overline{SP} = R\frac{\sin\theta_c}{\sin\theta_s} \tag{14}$$

$$r_2 = \overline{PQ} = 2R\cos\theta_2. \tag{15}$$

In addition, DF is the divergence factor, which can be calculated for the spherical surface as [11]

$$\mathrm{DF} = \frac{1}{\sqrt{1+\frac{r_2}{R_1}}}\frac{1}{\sqrt{\frac{1+r_2}{R_2}}} \tag{16}$$

$$R_1 = n\cos^2(\theta_2)\left(\frac{\cos^2\theta_1}{r_1} - \frac{n\cos\theta_2 - \cos\theta_1}{R}\right)^{-1} \tag{17}$$

$$R_2 = \left(\frac{1}{nr_1} - \frac{n\cos\theta_2 - \cos\theta_1}{nR}\right)^{-1}. \tag{18}$$

The electric and magnetic fields outside the spherical lens can then be represented by

$$\mathbf{E} = E_\parallel \hat{t}_r + E_\perp \hat{\phi} \tag{19}$$

$$\mathbf{H} = \hat{n}_t \times \mathbf{E}\sqrt{\frac{\varepsilon_0}{\mu_0}} \tag{20}$$

where $\hat{t}_r$ is the polarization of the parallel transmitted field, $\hat{\phi}$ is the polarization of the perpendicular transmitted field, and $\hat{n}_t$ is the direction of propagation of the transmitted field. As before, once the electric and magnetic fields have been found just outside the sphere, the corresponding equivalent electric and magnetic current densities can be calculated as

$$\mathbf{J} = \hat{r} \times \mathbf{H} = \left(-E_\parallel\hat{\theta} - \cos\theta_1 E_\perp \hat{\phi}\right)\sqrt{\frac{\varepsilon_0}{\mu_0}} \tag{21}$$

$$\mathbf{M} = -\hat{r} \times \mathbf{E} = E_\perp\hat{\theta} - \cos\theta_1 E_\parallel \hat{\phi}. \tag{22}$$

In the far field, the transverse electric field can be calculated using standard diffraction integrals over the closed spherical surface just outside the lens.

III. Spherical-Lens Characterization

The characterization strategy adopted in this study is to determine the optimum ratio d/R in terms of system radiation efficiency. The radius of the spherical lens is fixed to $R = 2.5$ cm, aiming at a system directivity of $D_{\mathrm{sys}} = 30$ dB at 77 GHz ($R/\lambda_0 = 6.5$). The system directivity is calculated from

$$D_{\mathrm{sys}} = \frac{4\pi U_{\max}}{P_{\mathrm{rad}}} \tag{23}$$

where $U_{\max}$ is the maximum radiation intensity and P_{rad} is the power radiated by the feed pattern. The corresponding system efficiency is defined as

$$\eta_{\mathrm{sys}} = \frac{D_{\mathrm{sys}}}{\left(\frac{2\pi R}{\lambda_0}\right)^2}. \tag{24}$$

The system efficiency can be decomposed according to $\eta_{\mathrm{sys}} = \eta_r\eta_s\eta_t$, where η_s is the spillover efficiency, η_r is the reflection efficiency through the spherical lens, and η_t is the taper efficiency over the spherical lens. These efficiencies can be calculated by

$$\eta_s = \frac{P_{\mathrm{in}}}{P_{\mathrm{rad}}} \tag{25}$$

$$\eta_r = \frac{P_{\mathrm{tr}}}{P_{\mathrm{in}}} \tag{26}$$

$$\eta_t = \frac{\frac{4\pi U_{\max}}{P_{\mathrm{tr}}}}{\left(\frac{2\pi R}{\lambda_0}\right)^2} \tag{27}$$

where P_{in} and P_{tr} are the incident power on the spherical-lens surface and the transmitted power through the spherical-lens surface, respectively.

Teflon Lenses: Fig. 4 presents the simulated system efficiency and its breakdown as a function of d/R for Teflon spherical lenses ($\varepsilon_r = 2.08$). Three different feed patterns with $m = 5, 9$, and 16 are used corresponding to −10-dB beamwidths of 100°, 80°, and 60°, respectively. The optimum d/R, which yields the best system efficiency, is 0.3–0.4, and the corresponding system efficiencies for feed beamwidths of 100°, 80°, and 60° are 51%, 54%, and 52%, respectively. The maximum system efficiency is achieved with a feed beamwidth of 80° and represents the best compromise between the taper and spillover efficiencies. The reflection efficiency is better than 90% due to the low dielectric constant of the Teflon, indicating that an antireflection coating is not necessary for most applications. Note that the 100°-beamwidth antenna results in optimal efficiency at $d/R = 0.3$ due to the rapid decline in its spillover efficiency.

Fig. 5 shows the 3-dB beamwidth and first sidelobe level of the far-field radiation pattern from the Teflon spherical lens. As expected, a wider feed pattern results in a higher taper efficiency, leading to a narrower beamwidth and a higher sidelobe level.

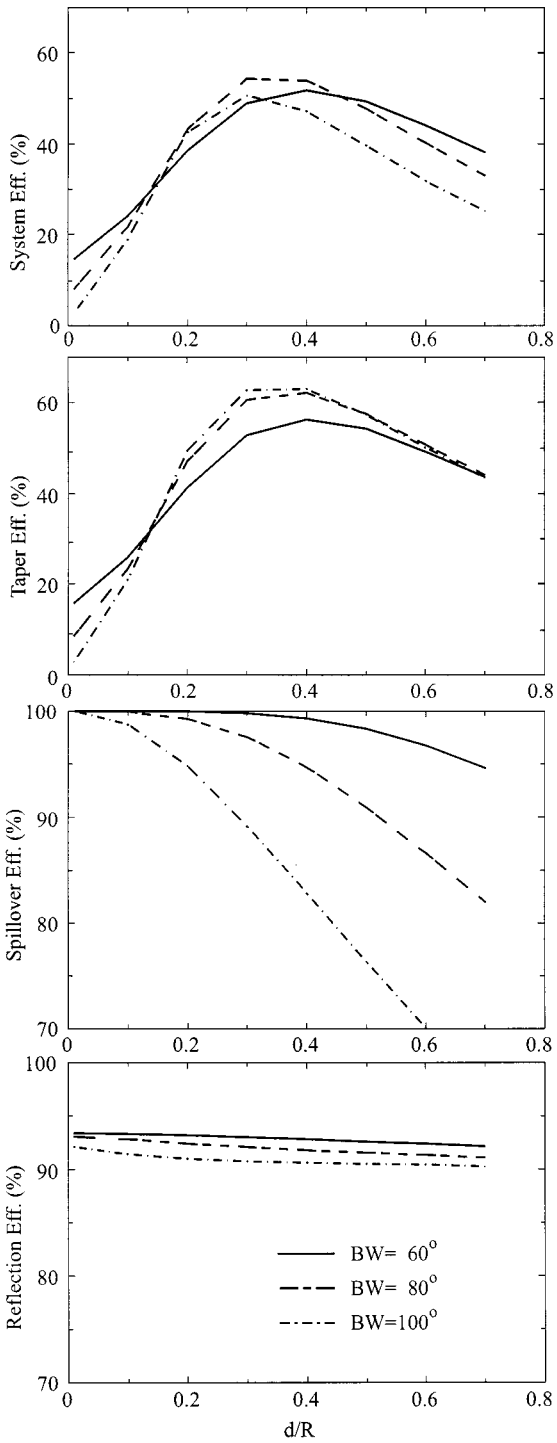

Fig. 4. Efficiency breakdown of a Teflon spherical lens for different beamwidths of the feed antenna.

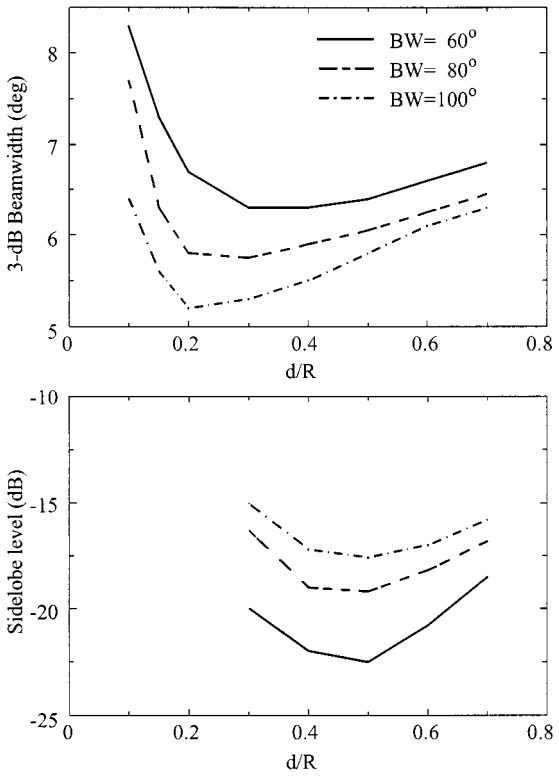

Fig. 5. 3-dB beamwidth and first sidelobe level as a function of d/R of a Teflon spherical lens for different beamwidths of the feed antenna.

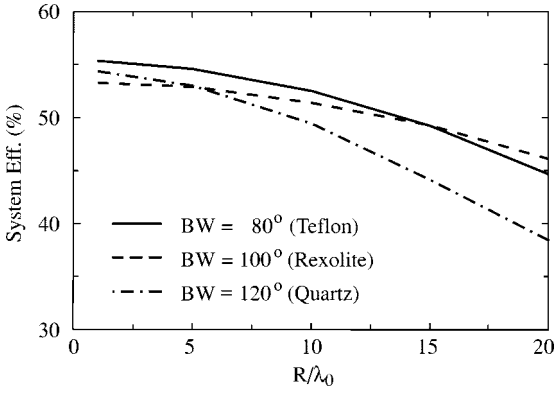

Fig. 6. System efficiency as a function of R/λ_0 of a spherical lens for different materials and their associated optimum feed beamwidth.

The focal point of the lens may be defined as the feed point that yields diffraction-limited patterns, i.e., a flat phase within the main lobe and a phase reversal in the sidelobes. This is observed at $d/R = 0.5$ for all three cases and, therefore, the spherical lens has a shorter focal length for antenna applications than what paraxial optics would predict ($d/R = 0.63$). Another way to determine the diffraction-limited position is to find the position that yields the lowest sidelobe level (Fig. 5). However, a lens with the feed placed at the diffraction-limited position does not necessarily imply an optimum efficiency due to the effect of the spillover loss. An excellent compromise between diffraction-limited performance and maximum efficiency is achieved at $d/R = 0.4$ for feed antennas with an 80° −10-dB beamwidth.

The spherical lens does not have a constant focus, as seen in Fig. 1. As a result, the system efficiency will depend on the radius of the spherical lens since the phase distribution on a spherical surface is different for lenses with different radii. Fig. 6 shows the system efficiency of the Teflon spherical lens as a function of R/λ_0, with the feed placed at $d/R = 0.4$. The spillover and reflection efficiencies remain constant with the radius R. It is clear from Fig. 6 that Teflon spherical lenses with a diameter larger than 30–40 λ_0 should be avoided [9].

It is interesting to investigate the effects associated with the phase of the feed pattern. This is especially important for the ta-

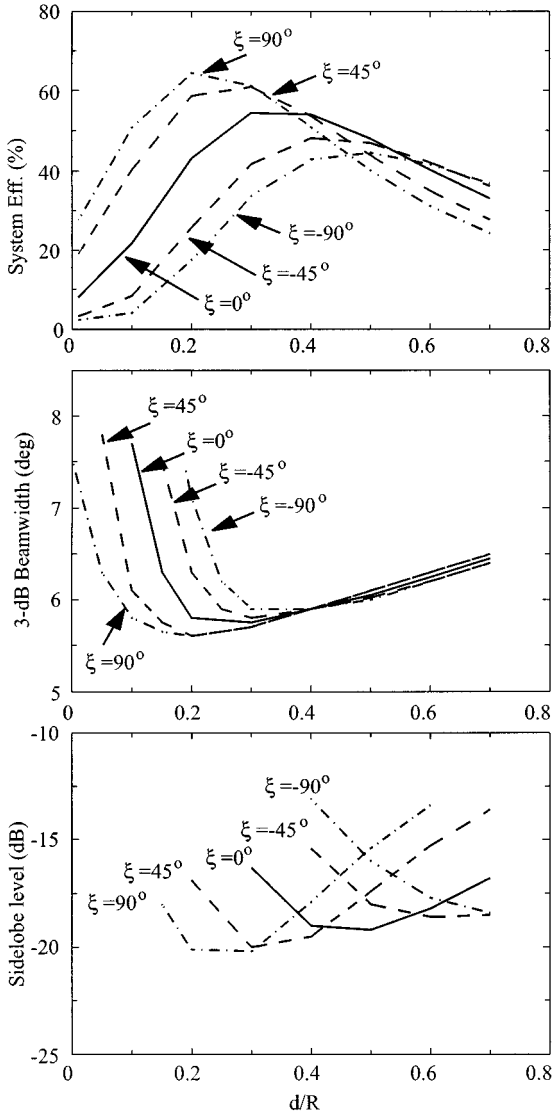

Fig. 7. Effects of the phase of the feed pattern on efficiency, 3-dB beamwidth, and sidelobe level for a Teflon spherical lens and a feed pattern beamwidth of 80°.

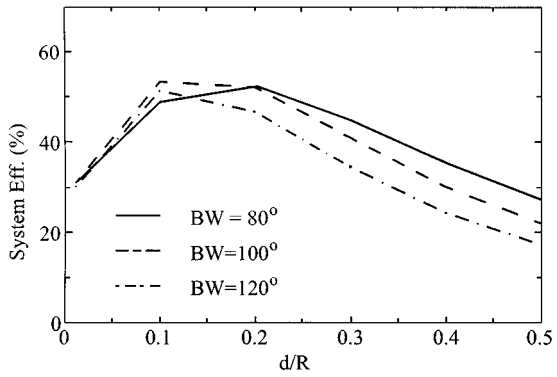

Fig. 8. System efficiency of a Rexolite spherical lens as a function of d/R for different beamwidths of the feed pattern.

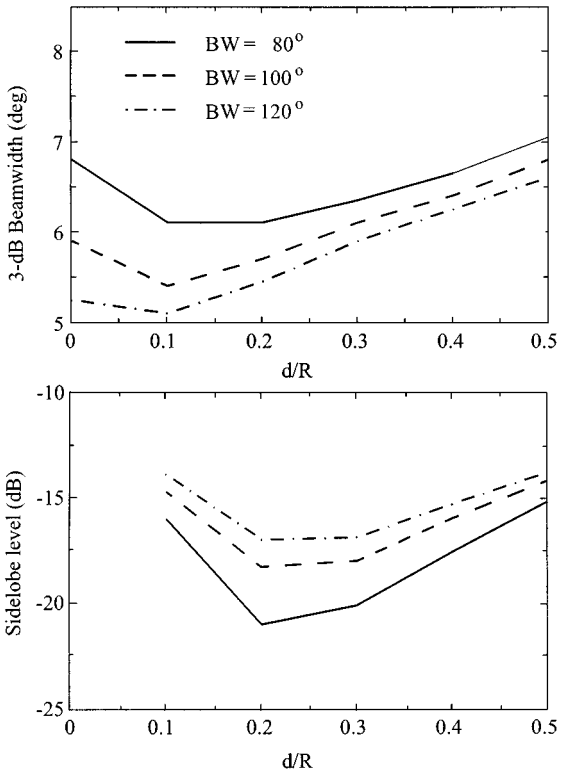

Fig. 9. 3-dB beamwidth and first sidelobe level as a function of d/R of a Rexolite spherical lens for different beamwidths of the feed antenna.

pered-slot antenna. For this purpose, an extra phase distribution is introduced in the feed pattern

$$E^{s'}_{\theta,\phi} = e^{A\sin\theta} E^{s}_{\theta,\phi} \tag{28}$$

where $E^{s}_{\theta,\phi}$ is defined in (5) and (6) and A is a constant used to control the phase error. Fig. 7 shows the system efficiency, 3-dB beamwidth, and the first sidelobe level for an 80° beamwidth feed antenna with various phase errors ξ defined at the -10-dB level. Accordingly, the constant A can be written as

$$A = \frac{\xi}{\sin\theta_{-10\text{dB}}} \tag{29}$$

where $\theta_{-10\text{dB}}$ is the elevation angle that corresponds to the -10-dB level in the feed pattern.

The spillover and reflection efficiencies are independent of the feed phase. The results clearly indicate that a positive phase distribution of the feed pattern can partly compensate for spherical aberration, leading to a better overall performance. This also results in a reduced optimum feed distance, leading to a more compact system. However, a positive phase distribution does not correspond to any practical feed antenna since it actually implies a focused beam incident on the lens. Unfortunately, most planar antennas have a negative phase distribution and should be limited to $\xi = -45°$ if good performance is desired.

Rexolite and Quartz Lenses: Figs. 8 and 9 show the simulated system efficiency and beamwidth as a function of d/R for a Rexolite spherical lens ($\varepsilon_r = 2.54$). The feed patterns use $m = 3, 5, 9$ corresponding to -10-dB beamwidths of 120°, 100°, and 80°. The optimum d/R is 0.1–0.2 for the best system efficiency. The reflection efficiency is 0.87–0.90 for all three cases. The corresponding system efficiencies for feed beamwidths of

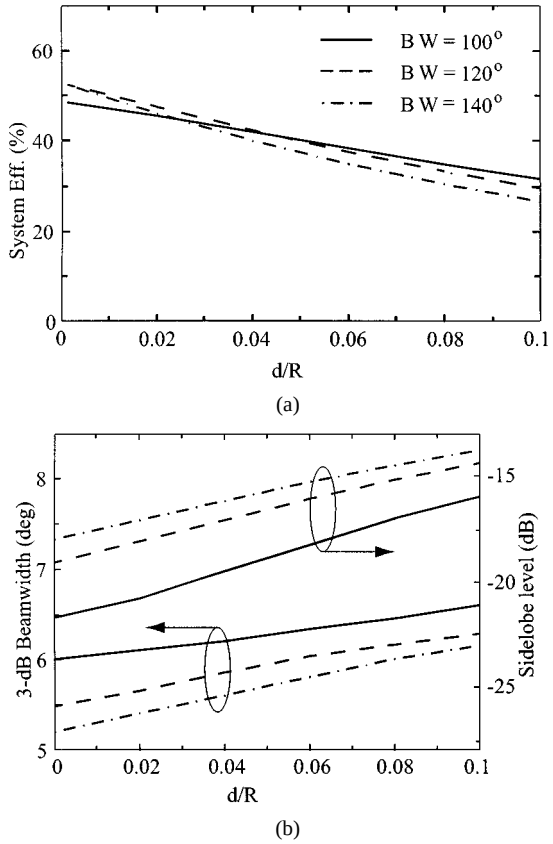

Fig. 10. (a) System efficiency and (b) 3-dB beamwidth and sidelobe level as a function of d/R for a quartz spherical-lens antenna for different beamwidths of the feed antenna.

TABLE I
COMPARISON OF TEFLON, REXOLITE, AND QUARTZ SPHERICAL LENSES. ALL DATA IS FOR OPTIMUM SYSTEM EFFICIENCY

	Teflon ($\varepsilon_r = 2.08$)	Rexolite ($\varepsilon_r = 2.54$)	Quartz ($\varepsilon_r = 3.78$)
d/R	0.4 - 0.5	0.16 - 0.2	0.0
Feed Beamwidth	80°	100°	120°
Efficiency (%)	54	55	52
Beamwidth	5.7 - 5.8°	5.6 - 5.7°	5.5°
Sidelobe level (dB)	-19	-18	-18
Maximum R/λ_0	20	20	14

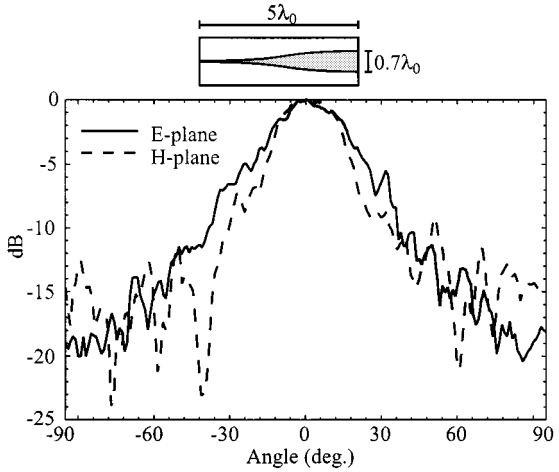

Fig. 11. Measured E- and H-plane patterns of the tapered slot antenna on a 5-mil Duroid substrate.

120°, 100°, and 80° are 52%, 55%, and 53%, respectively. The diffraction-limited pattern occurs at $d/R = 0.2$ for all feed antennas. Therefore, a position of $d/R = 0.16$–0.2 results in excellent performance for a feed beamwidth of 100° and the Rexolite lens leads to a more compact structure than the Teflon lens. However, it is more expensive to build and has a higher dielectric loss at millimeter-wave frequencies.

Fig. 10(a) shows the simulated system efficiency for a quartz spherical lens ($\varepsilon_r = 3.78$) with the feed patterns of 140°, 120°, and 100° ($m = 2, 3, 5$). Notice that the focal point is just outside the lens ($d/R = 0$). The optimum system efficiency is 52% for a 120° beamwidth. The reflection loss is 78% for the 120° feed pattern. As shown in Fig. 3, diffraction-limited pattern for all three feed patterns occurs at a position at $d/R = 0.0$.

The effects of a phase distribution in the feed pattern for a Rexolite or a quartz lens are similar to the Teflon lens. The system efficiency can be improved by using a feed with positive phase distribution. However, if a feed antenna with a negative phase distribution is used, then the phase error should be kept at below $-45°$ (Rexolite) and $-90°$ (quartz) at the -10-dB level. Detailed calculations are presented in [12]. Finally, Fig. 6 shows that one can use Rexolite and quartz lenses up to a maximum of $R/\lambda_0 = 14$–20. The system efficiency drops quickly at larger R/λ_0 due to spherical aberrations.

A comparison between Teflon, Rexolite, and quartz spherical lenses is shown in Table I. All lenses exhibit similar efficiency and beamwidths when well designed. The quartz lens presents the limiting case ($d/R = 0$) and, therefore, results in the most compact system, but is very expensive to produce. A Teflon or Rexolite lens is an excellent compromise for millimeter-wave applications.

IV. MEASUREMENTS ON A SINGLE ELEMENT

The feed antenna is an endfire tapered slot antenna with parameters given in Fig. 11. This antenna has been developed by Sugawara *et al.* and has been scaled for 77-GHz applications [13], [14]. The antenna is fabricated using standard lithography and copper etching on a 127-μm-thick Duroid substrate with $\varepsilon_r = 2.2$. A slot-line to microstrip transition is fabricated at the end of the tapered-slot antenna and a planar Schottky diode (Metelics MSS 30–154-B10 or Agilent 1GG5–4002) is used as the millimeter-wave video detector. The transmitted signal from a Gunn diode is modulated at 1 kHz and the detected video signal is sent to a lock-in amplifier. The signal-to-noise ratio is limited by the measurement chamber, the linearity of the lock-in amplifier and the diode responsivity and is 33–36 dB at 77 GHz. The measured feed patterns are shown in Fig. 11 and result in a -10-dB beamwidth of 74° in the E-plane and 67° in the H-plane patterns. The cross-polarization levels are lower than -10 dB.

The far-field pattern of the tapered slot antenna can be modeled with (2) using $m = 10$, which results in a -10-dB beamwidth of 75°. Fig. 12 compares the simulated and measured radiation patterns of a spherical Teflon lens with $R = 2.5$ cm ($R/\lambda_0 = 6.52$) fed by the endfire tapered slot antenna. The lens is fabricated using a standard CNC milling

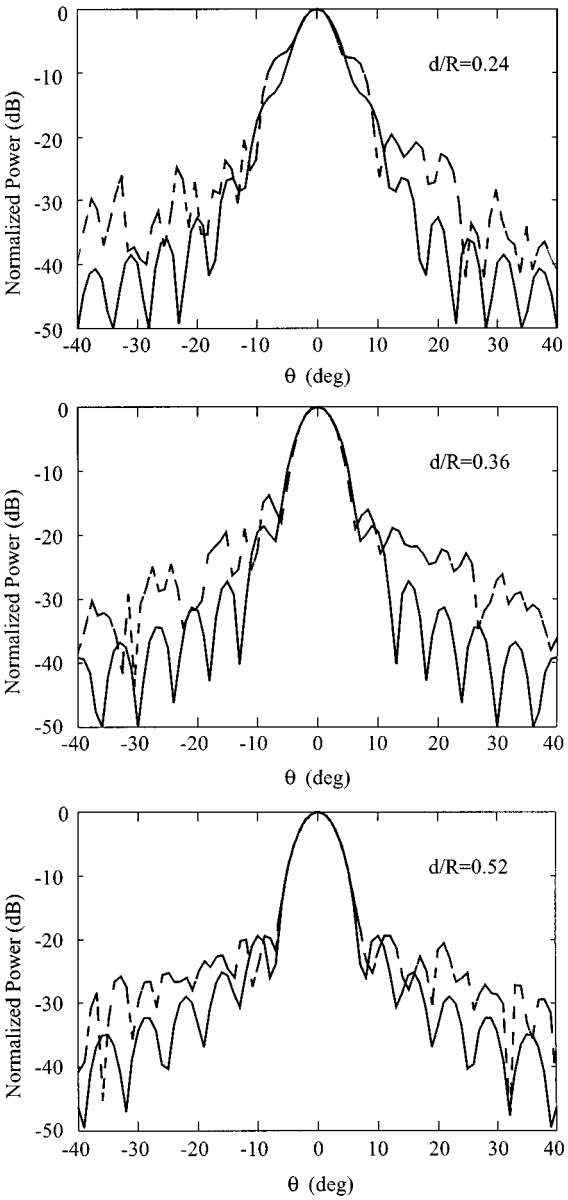

Fig. 12. Comparison of simulated (—) and measured (- - -) E-plane radiation patterns at 77 GHz for a Teflon spherical lens with $R = 2.5$ cm for different d/R.

machine, with a surface roughness smaller than $\lambda/15$. A distance of 1–2 mm (estimated) from the edge of the tapered slot antenna to its phase center is included in the distance d. As shown, the measurements agree very well with the simulations. Diffraction-limited patterns (deepest nulls) occur at a relative distance d/R of approximately 0.52, which compares well to the expected d/R of 0.5 (see Fig. 5). The main beam and first sidelobe level are accurately predicted for d/R values greater than 0.36. The inaccuracy for small d/R values can be attributed to near-field effects of the feed antennas or to the disturbed feed pattern caused by the proximity of the spherical lens. The disagreement for higher order sidelobes is due to the approximate feed patterns used and also to the fact that only first-order ray tracing has been taken into account.

The measured E- and H-plane patterns for $d = 13$ mm ($d/R = 0.52$) are shown in Fig. 13. It is seen that the tapered-slot antenna/spherical Teflon lens design results in excellent E- and H-plane patterns, with a -10-dB beamwidth of 10.6°, a sidelobe level below -20 dB, and a cross-polarization levels below -19 dB at the diffraction limited position.

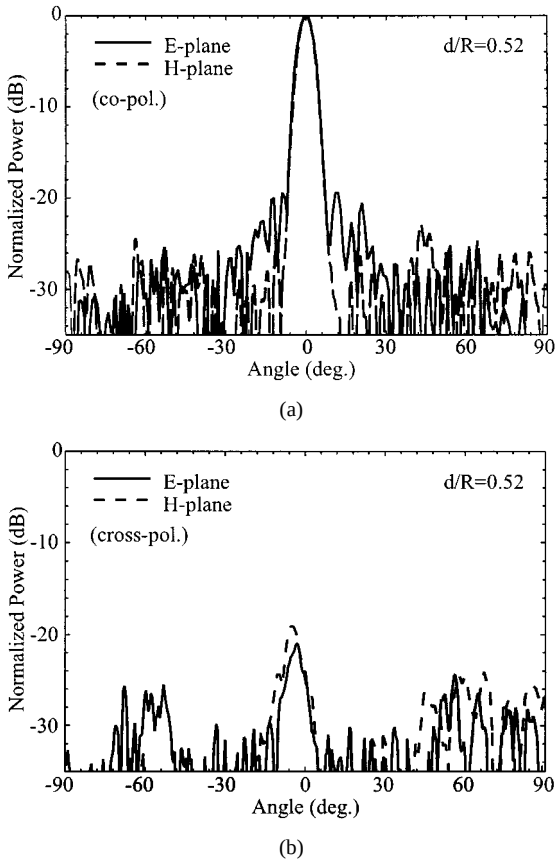

Fig. 13. Measured E- and H-plane patterns at 77 GHz of a Teflon spherical lens with $R = 2.5$ cm fed with a tapered-slot antenna. (a) Co-polarization. (b) Cross-polarization.

Absolute Gain Measurements: The absolute gain of the $R = 2.5$ cm spherical-lens antenna was measured using the standard-gain technique (with a calibrated transmitting horn antenna) and the Friis formula. The tapered slot antenna is replaced by a small pyramidal waveguide horn with an aperture of $2.7\lambda_0 \times 1.9\lambda_0$ to result in a -10-dB beamwidth of 70°. The transmitted power from the Gunn diode and the received power were both measured using a power meter.

The measured radiation patterns of the horn/spherical lens are nearly identical to Fig. 13 and will not be repeated. The measured gain G_m and efficiency versus position are shown in Fig. 14. The efficiency is defined as G_m/D, where $D = 4\pi A/\lambda^2$ is the maximum directivity of the lens aperture.

As seen in Fig. 14, the measured efficiency agrees fairly well with theory. Differences can be explained by the loss in the Teflon lens, which was not taken into account in the calculations. The absorption coefficient of Teflon at 77 GHz is around 0.012 Np · cm [15], which results in a loss of around 0.5 dB. Also, the location of the phase center of the horn may be the reason for additional deviations.

Radiometer Efficiency Measurements: The efficiency of the spherical-lens antenna was measured using radiometer techniques (Fig. 15). This technique has been described in

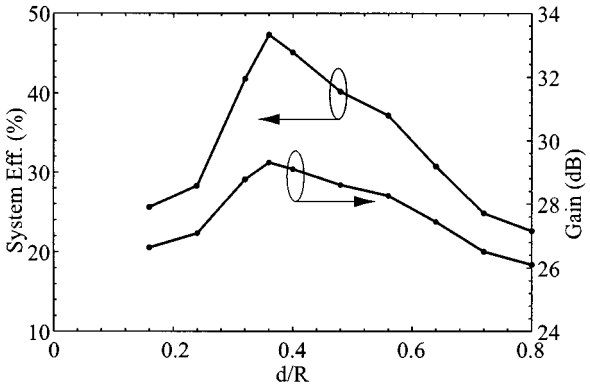

Fig. 14. Measured gain and system efficiency of a Teflon spherical lens fed using a small pyramidal horn.

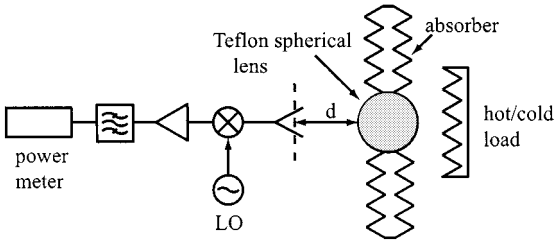

Fig. 15. Setup for efficiency measurement using radiometer techniques.

[16] and is accurate to within $\pm 5\%$. The radiometer method estimates the spillover, dielectric absorption, and reflection loss of the spherical-lens antenna. It does not take into account the taper and phase-loss efficiency since the hot/cold absorber will always couple to the antenna using whatever mode for maximum power transfer.

The small pyramidal waveguide horn is used for the feed antenna and is coupled directly to the balanced mixer/radiometer. The measured efficiency was 82 $\pm$5%, which is in agreement with the calculations of Fig. 4.

V. Multibeam Array

A top and side view of the 77-GHz multibeam array is shown in Figs. 16 and 17. The tapered slot antennas are placed on the $d = 13$ mm arc with a center-to-center spacing of 3.6 mm. This results in a beam scan of 5.5° between any two antenna elements and, therefore, the pattern crossover should occur at the -3.5-dB level. A total of 33 antennas are needed to cover the 180° scan angle and the measured patterns are shown in Fig. 18. The patterns are actually measured from 0° to 90° for a total of 17 patterns and the data is reflected about 0° to show the $\pm 90^\circ$ coverage. The peak detected powers were within ± 1.5 dB from each other up to the $\pm 75^\circ$ scan angle and are all normalized to 0 dB. This is acceptable since different Schottky diodes are used at each antenna. However, there was a distinct drop in the measured power level for the three edge elements on either side of the array, as shown in Fig. 18. The reason is that the 33-beam antenna array was mounted on a thick metal platform (400 μm), which resulted in a lot of scattering for scan angles greater than 75° (Fig. 17). The sidelobe level remains below -16 dB up to the $\pm 80^\circ$ scan angle.

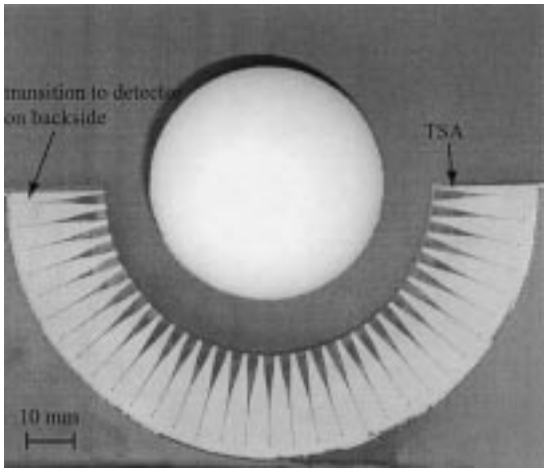

Fig. 16. 33-beam array with Teflon spherical lens resulting in a -3.5-dB crossover of adjacent beams.

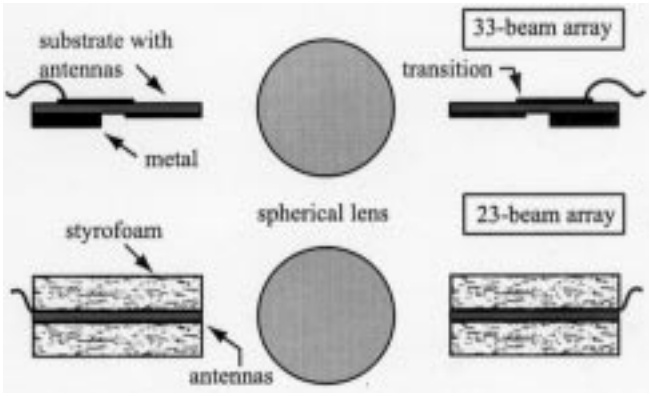

Fig. 17. Different ways of mounting the 33- and 23-beam array.

A tapered-slot-antenna design with a center-to-center spacing of 5.2 mm was also measured at 77 GHz. In this case, a total of 23 antennas are needed to cover the 180° scan angle and the pattern crossover occurs at the -6-dB level. The 23-beam array was mounted between two thick Styrofoam layers ($\varepsilon_r \simeq 1.05$) (Fig. 17), which resulted in minimal scattering at large scan angles. The patterns were again measured from 0° to 90° (12 beams) and "reflected" about 0° for $\pm 90^\circ$ coverage. The detected signal varied by ± 1.5 dB randomly up to the 90°-scan antenna. The antennas do not scatter even if looking straight at each other. This is because once the power is radiated from antenna 1 (see Fig. 19) through the lens, the electromagnetic field is almost like a plane wave and only a very small portion couples to antenna 23. To our knowledge, this performance is not yet attainable using any antenna design at millimeter-wave frequencies.

VI. Elevation-Scan Measurements

The tapered-slot antenna can be displaced *linearly* in the vertical direction to result in a tilted beam in the elevation direction. The reason for the linear and not radial displacement is that horizontal antenna "cards" can then be used for elevation scanning. The measured patterns (see Fig. 20) indicate that one can obtain an elevation scan of up to 11°–17° for a displacement of

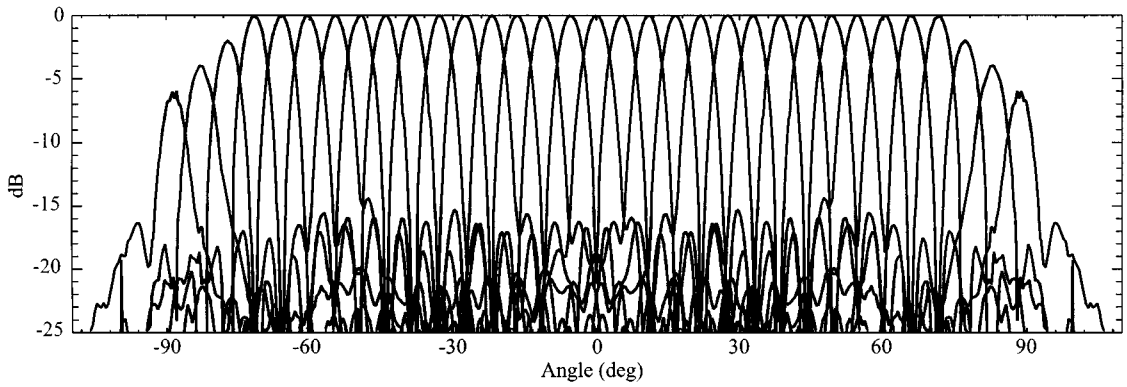

Fig. 18. Measured E-plane patterns of the 33-beam array with a crossover of -3.5 dB. The drop in signal for the last three antennas is due to the mounting setup.

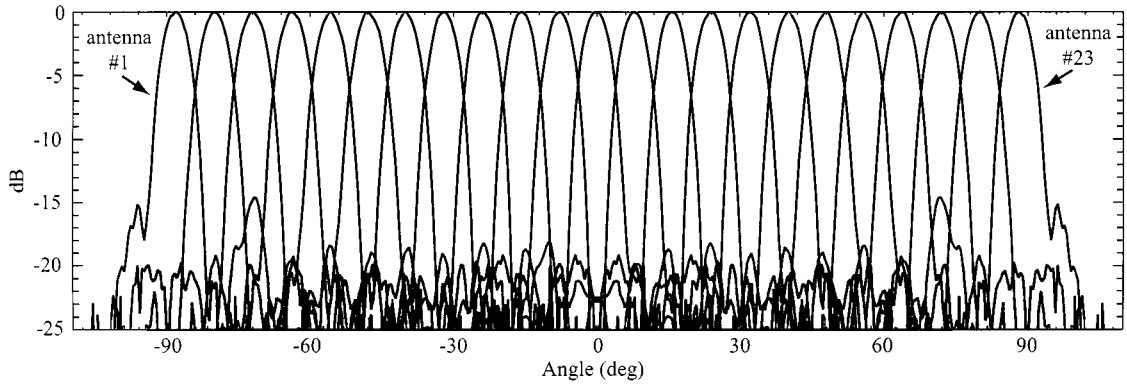

Fig. 19. Measured E-plane patterns of the 23-beam array with a crossover of -6 dB. The peak levels are all within ± 1.5 dB of each other, including the patterns of antennas #1 and #23.

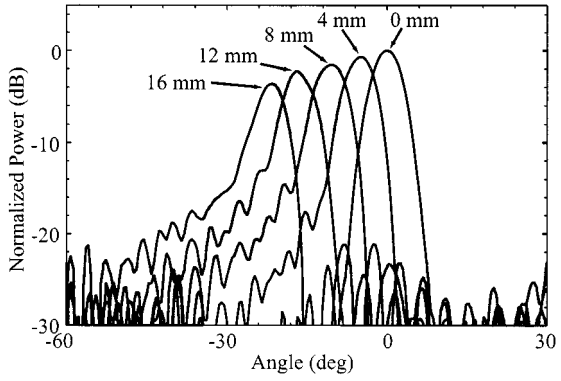

Fig. 20. Measured H-plane patterns of single antenna element with Teflon spherical lens as a function of vertical offset of feed antenna with respect to the lens.

8–12 mm while still maintaining excellent patterns. The associated gain loss is around 2.0 dB. Of course, if the feed antenna is displaced radially in the vertical direction, then the patterns are identical to Fig. 13 due to the symmetry of the lens.

VII. Conclusion

This paper has presented an accurate analysis of the spherical-lens antenna system. The analysis was based on a combined ray optics/diffraction method. A single lens system was used, but the analysis can be easily extended to include a dual-shell system (i.e., a matching layer on the lens surface). It was seen that Teflon, Rexolite, or quartz lenses, when well designed, result in nearly the same efficiency, beamwidth, and sidelobe levels. It was also found that the "diffraction-limited" feed position for antenna applications is closer to the lens than the paraxial focus predicted using ray optics, but is farther than the position for optimum system efficiency. For the Teflon case, the maximum useful spherical-lens diameter was 30–$40\lambda_0$ and resulted in a 3-dB beamwidth of 1.9°–1.4° and maximum directivity of 39.5–42.0 dB. The corresponding maximum gain was 37.5 dB for a diameter of $40\lambda_0$, taking into account the system efficiency for large R/λ_0 (Fig. 6) and the Teflon dielectric loss [15]. The analysis did not take into account the multiple reflections inside the spherical lens and, therefore, cannot accurately predict the far sidelobe levels. Still, the measured patterns, gains, and efficiency agree very well with measurements at 77 GHz.

The spherical Teflon lens system is also used in a low-cost multibeam system using endfire tapered-slot antennas. The measured patterns show that the system results in an extremely wide scan angle with virtually no gain loss (up to $\pm 90°$). Elevation scan measurements indicate that one can *linearly* displace the array up to 10 mm and result in an elevation scan of 13° with only 2.0 dB of gain loss. This is an excellent low-cost solution for multibeam wide scan-angle systems, which need to image in the vertical direction for $\pm 10°$.

REFERENCES

[1] I. Gresham, N. Jain, T. Budka, A. Alexanian, N. Kinayman, B. Ziegner, S. Brown, and P. Staecker, "A compact manufactureable 76–77-GHz radar module for commercial ACC applications," *IEEE Trans. Microwave Theory Tech.*, vol. 49, pp. 44–58, Jan. 2001.

[2] K. K. Chan, S. K. Ral, G. A. Morin, and M. Q. Tang, "Triangular ray-tube analysis of dielectric lens antennas," *IEEE Trans. Antennas Propagat.*, vol. 45, pp. 1277–1285, Aug. 1997.

[3] F. Demmerle, S. Kern, and W. Wiesbeck, "A bi-conical multibeam antenna for space division multiple access," in *IEEE AP-S Int. Symp. Dig.*, Montreal, QC, Canada, Aug. 1997, pp. 1082–1085.

[4] J. Sanford, "A Luneberg-lens update," *IEEE Antennas Propagat. Mag.*, vol. 37, pp. 76–79, Jan. 1994.

[5] R. K. Luneburg, *The Mathematical Theory of Optics*. Providence, RI: Brown Univ. Press, 1994.

[6] H. Mosallaei and Y. Rahmat-Samii, "Nonuniform Luneburg and two-shell lens antennas: Radiation characteristics and design optimization," *IEEE Trans. Antennas Propagat.*, vol. 49, pp. 60–68, Jan. 2001.

[7] G. T. d. Francia, "Spherical lenses for infrared and microwaves," *J. Appl. Phys.*, vol. 32, pp. 2051–2051, 1961.

[8] T. L. A. Rhys, "The design of radially symmetric lenses," *IEEE Trans. Antennas Propagat.*, vol. AP-18, pp. 497–506, July 1970.

[9] G. Bekefi and G. W. Farnell, "A homogeneous dielectric sphere as a microwave lens," *Can. J. Phys.*, vol. 34, pp. 790–803, 1956.

[10] L. C. Gunderson, "An electromagnetic analysis of a cylindrical homogeneous lens," *IEEE Trans Antennas Propagat.*, vol. AP-20, pp. 476–479, July 1972.

[11] S. Lee, M. S. Sheshadri, V. Jamnejad, and R. Mittra, "Refraction at a curved dielectric interface: Geometrical optics solution," *IEEE Trans. Microwave Theory Tech.*, vol. MTT-30, pp. 12–19, Jan. 1982.

[12] X. Wu, "Millimeter-wave lens antennas for broadband wireless communications and automobile collision avoidance," Ph.D. dissertation, Dept. Elect. Eng., Univ. Toronto, Toronto, ON, Canada, 2001.

[13] S. Sugawara, Y. Maita, K. Adachi, K. Mori, and K. Mizuno, "A mm-wave tapered slot antenna with improved radiation pattern," in *IEEE MTT-S Int. Microwave Symp. Dig.*, Anaheim, CA, June 1999, pp. 1151–1154.

[14] K. S. Yngvesson, T. L. Korzeniowski, Y. S. Kim, E. L. Kollberg, and J. F. Johansson, "The tapered slot antenna—A new integrated element for mm-wave applications," *IEEE Trans. Microwave Theory Tech.*, vol. 37, pp. 365–374, Feb. 1989.

[15] M. N. Afsar, "Dielectric measurements of common polymers at millimeter wavelength range," in *IEEE MTT-S Int. Microwave Symp. Dig.*, 1985, pp. 439–442.

[16] J. Ahkenazy, E. Levine, and D. Treves, "Radiometric measurement of antenna efficiency," *Electron. Lett.*, vol. 21, no. 3, pp. 111–112, Jan. 1985.

[17] E. Hecht, *Optics*, 2nd ed. Reading, MA: Addison-Wesley, 1987.

Bernhard Schoenlinner (S'00) was born in Trostberg, Germany, in 1973. He received the Dipl.-Ing. degree from the Technische Universität München, Munich, Germany, in 2000, and is currently working toward the Ph.D. degree in electrical engineering from The University of Michigan at Ann Arbor.

His research interests are microwave and millimeter-wave circuits and devices. His work focuses on millimeter-wave radar systems including the application of microelectromechanical-system (MEMS) switches.

Xidong Wu (S'91) was born in Wuxi, China, in 1970. He received the B.S. degree from Southeast University, Nanjing, China, in 1989, the M.A.Sc. degree from the University of Toronto, Toronto, ON, Canada, in 1996, both in electrical engineering, and is currently working toward the Ph.D. degree in electromagnetics at the University of Toronto.

His current research interests include millimeter-wave integrated-circuit antennas, smart antennas for broad-band wireless communications, millimeter-wave circuit design, and numerical electromagnetics.

Jim P. Ebling received the B.S.E.E.E. degree from the University of Michigan at Dearborn, in 1983.

In 1981, he joined the Environmental Research Institute of Michigan (ERIM), as a cooperative education student, where he performed simulation analysis for airborne synthetic aperture radar (SAR) systems. He then joined the Electronics Development Department, University of Michigan at Dearborn, where he performed digital design and development of SAR subsystems and support equipment. He later became involved in design and development of RF and microwave subsystems, and performed radar system design, analysis, and program management. In 1994, he joined Canopus Systems Inc., Ann Arbor, MI, where he designed and developed space-based accelerometry systems for the characterization of the microgravity environment on various space vehicles, including the Space Shuttle and the International Space Station. He participated in development efforts of a microelectromechanical system (MEMS)-based system with sub micro-g sensitivity. Since 1997, he has been pursuing research interests in radar system design for the transportation industry.

George V. Eleftheriades (S'86–M'88–SM'02) received the Ph.D. and M.S.E.E. degrees in electrical engineering from The University of Michigan at Ann Arbor, in 1993 and 1989, respectively, and the Diploma (with distinction) in electrical engineering from the National Technical University of Athens, Athens, Greece, in 1988.

From 1994 to 1997, he was with the Swiss Federal Institute of Technology, Lausanne, Switzerland, where he was engaged in the design of millimeter and submillimeter-wave receivers and in the creation of fast computer-aided design (CAD) tools for planar packaged microwave circuits. In 1997, he joined the Department of Electrical and Computer Engineering, University of Toronto, Toronto, ON, Canada, where he is currently an Assistant Professor. He has authored or coauthored over 60 papers in refereed journals and conference proceedings. His current research activities include millimeter-wave integrated-circuit antennas and components for broad-band wireless communications, low-loss micromachined components for Ka-band satellite communications, sub-millimeter-wave radiometric receivers, electromagnetic design for high-speed digital circuits, and novel electromagnetic meta-materials.

Dr. Eleftheriades was a corecipient of the 1990 Best Paper Award presented at the 6th International Symposium on Antennas (JINA), the 1992 Student Paper Award presented at the IEEE Antennas and Propagation Society (IEEE AP-S) Symposium, and the 1991 Distinguished Achievement Award presented by The University of Michigan at Ann Arbor. He was also the recipient of the 2001 Gordon Slemon Teaching Award presented by the University of Toronto and the 2001 Ontario Premier Research Excellence Award.

Gabriel M. Rebeiz (S'86–M'88–SM'93–F'97) received the Ph.D. degree in electrical engineering from the California Institute of Technology, Pasadena, in 1988.

In September 1988, he joined the faculty of The University of Michigan at Ann Arbor, and was promoted to Full Professor in 1998. He held short visiting professorships at the Chalmers University of Technology, Göteborg, Sweden, Ecole Normale Superieur, Paris, France, and Tohoku University, Sendai, Japan. His research interests include applying micromachining techniques and MEMS for the development of novel components and subsystems for radars and wireless systems. He is also interested in Si/GaAs RF integrated circuit (RFIC) design for receiver applications, and in the development of planar antennas and microwave/millimeter-wave front-end electronics for communication systems, automotive collision-avoidance sensors, monopulse tracking systems, and phased arrays.

Prof. Rebeiz was the recipient of the 1991 National Science Foundation Presidential Young Investigator Award and the 1993 URSI International Isaac Koga Gold Medal Award for Outstanding International Research. He was also the recipient of the 1995 Research Excellence Award presented by The University of Michigan at Ann Arbor. Together with his students, he was the recipient of Best Student Paper Awards of the IEEE Microwave Theory and Techniques Society (IEEE MTT-S) (1992, 1999-1994), and the IEEE Antennas and Propagation Society (IEEE AP-S) (1992, 1995). He was also the recipient of the 1990 *Journées Int. de Nice sur les Antennes* (*JINA*) Best Paper Award, and the 1997 University of Michigan Electrical Engineering and Computer Science (EECS) Department Teaching Award. He was selected by his students as the 1997–1998 Eta Kappa Nu EECS Professor of the Year. He was also the recipient of the 1998 College of Engineering Teaching Award and the 1998 Amoco Foundation Teaching Award, given yearly to one faculty member of The University of Michigan at Ann Arbor for excellence in undergraduate teaching. He was the corecipient of the IEEE 2000 Microwave Prize for his work on MEMS phase shifters.